Accepted manuscript:

Mobilization and isotope fractionation of chromium during water-rock interaction in presence of siderophores

by

Dennis Kraemer[a,*], Robert Frei[b], Sebastian Viehmann[a,c], Michael Bau[a]

[a] Department of Physics and Earth Sciences, Jacobs University Bremen, Campus Ring 1, 28759, Bremen, Germany
[b] Department of Geosciences and Natural Resource Management, University of Copenhagen, Øster Voldgade 10, 1350, Copenhagen, Denmark
[c] Department of Geodynamics and Sedimentology, University of Vienna, Althanstraße 14, 1090, Vienna, Austria

https://doi.org/10.1016/j.apgeochem.2019.01.007

Received 25 July 2018; Received in revised form 14 January 2019; Accepted 14 January 2019
Available online 17 January 2019 (Embargo 24 months)

Mobilization and Isotope Fractionation of Chromium during Water-Rock Interaction in Presence of Siderophores

Dennis Kraemer[1*], Robert Frei[2], Sebastian Viehmann[1,3] and Michael Bau[1]

[1] Department of Physics and Earth Sciences, Jacobs University Bremen, Campus Ring 1, 28759 Bremen, Germany

[2] Department of Geosciences and Natural Resource Management, University of Copenhagen, Øster Voldgade 10, 1350 Copenhagen, Denmark

[3] Department of Geodynamics and Sedimentology, University of Vienna, Althanstraße 14, 1090 Vienna, Austria

* email: d.kraemer@jacobs-university.de

Keywords: chromium isotopes, siderophores, DFOB, redox proxies, biomolecules

Abstract

Chromium mobilization and isotope fractionation during water-rock interaction in presence of the biogenic siderophore desferrioxamine B (DFOB) was studied with batch leaching experiments on chromitite and other igneous oxide and silicate rocks. Siderophores are a group of organic ligands synthesized and excreted by bacteria, fungi and plants to enhance the bioavailability of key nutrients like Fe. However, the DFOB siderophore also has a strong affinity for complexation with other metals such as Cr, U and rare earth elements. Here we show that leaching of rocks in the presence of the hydroxamate siderophore DFOB significantly increased the mobilization of Cr from all investigated rocks and caused an enrichment of the heavier ^{53}Cr isotope in leachates from chromitite ($\delta^{53}Cr_{leach}$ = +0.15 ± 0.087‰ to +2.14 ± 0.042 ‰) and from altered silicate rock ($\delta^{53}Cr_{leach}$ = +0.48 ± 0.07‰). In contrast, stable isotope fractionation of Cr was not observed in DFOB leachates of pristine silicate and low-Cr oxide rocks. Leaching in the presence of citric acid significantly enhanced Cr mobility, but did not result in fractionation of Cr isotopes. Chromium isotope fractionation is used in geochemistry as a quantitative proxy for oxidative weathering, because Cr(III) is oxidized

to Cr(VI) in presence of MnO_2 and the associated Cr isotope fractionation is commonly linked to the presence of oxygen in the atmosphere. Our findings indicate that the presence of specific biogenic ligands with a high affinity for Cr are also able to fractionate Cr isotopes. The presence of biomolecules like siderophores during weathering, hydrothermal alteration or during mineral precipitation, therefore, may put constraints on the applicability of certain trace metals and their isotopes as redox proxies in modern and past environments. The results of our study also suggest that siderophores may have a high potential for (bio)remediation of Cr-contaminated sites and detoxification of contaminated natural waters.

1. Introduction

Chromium occurs as Cr(III) and Cr(VI) redox species in the natural environment. While the former is rather immobile and non-toxic, the latter is mobile and considered toxic (Fendorf, 1995). Under present-day atmospheric conditions, Cr(VI) is the thermodynamically most stable redox species of Cr and, hence, Cr mobility is significantly increased during oxidative weathering. The mobile anionic species are chromate, CrO_4^{2-}, and bichromate, $HCrO_4^-$. The aqueous Cr(VI) species solubilised during weathering enters streams, rivers, and ultimately the ocean (Oze et al., 2007). Chromium is used in a variety of technological applications such as electroplating, dyeing and tanning, and as such, significant quantities are introduced into the environment as a contaminant. The mobile form, Cr(VI), is considered carcinogenic (Kortenkamp et al., 1996) and its input into groundwater and surface water may have serious effects on flora and fauna. Hence, the remediation of Cr-contaminated soils and natural waters is of utter importance. Remediation relies solely on the *in-situ* reduction of Cr(VI) to immobile Cr(III). Therefore, it is essential to understand the processes and effects that organisms and their extracellular exudates such as metal-specific organic ligands (siderophores/metallophores) and organic acids, have on Cr mobility and Cr oxidation/reduction in the environment. It has also been shown that plants and bacteria may play an important role in cleaning up Cr-contaminated sites by means of biosorption (Owlad et al., 2009; Veglio' and Beolchini, 1997) or microbially-mediated Cr reduction. Chromium can be reduced *in-situ* to Cr(III) by plants (Lytle et al., 1998) as well as by

63 bacteria, algae and fungi (e.g., Basu et al., 2014; Cervantes et al., 2001; Han et al., 2012;
64 Sikora et al., 2008). Bioremediation, therefore, may become an important future
65 technology for remediation of sites contaminated with Cr.

66 In aqueous systems, the mobile form, Cr(VI), is isotopically heavier in equilibrium and
67 enriched by about 7‰ in ^{53}Cr relative to ^{52}Cr (Schauble et al., 2004). Microbial reduction
68 of Cr(VI) to Cr(III) may produce Cr isotope ratios as low as -4.1 ‰ in the product of the
69 reduction reaction (Sikora et al., 2008), whilst abiogenic reduction may lead to a Cr
70 isotope fractionation ranging from -3.91±0.16‰ to -2.11±0.04‰ (Basu & Johnson, 2012).
71 In contrast, Cr(III) oxidation may result in Cr isotope ratios in the range of +0.2‰ to
72 +0.6‰ in presence of H_2O_2 (Zink et al., 2010) or up to +1‰ in presence of Mn dioxide
73 (Ellis et al., 2008). The stable Cr isotope system has received considerable interest in the
74 geochemistry community (Qin and Wang, 2017). Stable isotope ratios of chromium can
75 be used as indicators for microbial or abiotic Cr(VI) reduction in groundwater and to trace
76 Cr pollution in ground- and river water (Berna et al., 2010; Economou-Eliopoulos et al.,
77 2014; Izbicki et al., 2012; Wanner et al., 2012). In soil systems, MnO_2 usually acts as an
78 important oxidizer for Cr(III) (Kotaś and Stasicka, 2000; Palmer and Wittbrodt, 1991).
79 Deviations of the $\delta^{53}Cr$ signal from the bulk Earth ratio in marine chemical and epiclastic
80 sediments and in paleosols are used as proxies for the presence of free oxygen in the
81 Earth's surface system. This may help to evaluate local redox-conditions of ancient
82 environments and the redox-evolution of Early Earth (e.g., Arcy et al., 2016; Babechuk et
83 al., 2017; Canfield et al., 2018; Cole et al., 2016; Crowe et al., 2013; Frei et al., 2016,
84 2009; Frei and Rosing, 2005; Gilleaudeau et al., 2016; Holmden et al., 2016; Huang et
85 al., 2018; Planavsky et al., 2014; Rodler et al., 2017; Wang et al., 2016). However, the
86 applicability of Cr isotope fractionation as a paleo-redox proxy is largely based on the
87 assumption that oxidative weathering is the sole producer of heavy Cr isotope enrichment
88 in weathering solutions. Recent studies have questioned this assumption.
89 Serpentinization, for example, leads to Cr oxidation even at low oxygen fugacities (Oze et
90 al., 2016) and ligand-promoted dissolution of Cr(III) (hydr)oxides also facilitates significant
91 Cr isotope fractionation (Saad et al., 2017b). Further research, therefore, needs to
92 investigate whether other mechanisms exist, that produce Cr isotope fractionation in
93 anoxic environments where it is commonly attributed to the presence of oxygen.

Here we report on the influence of certain biomolecules, siderophores, on Cr mobilization and Cr isotope fractionation from igneous rocks. Siderophores (also referred to as metallophores; Kraemer *et al.*, 2014) are a group of natural organic ligands produced by a wide range of bacteria, plants and fungi to mobilize and bind trivalent Fe from sparingly soluble mineral structures and thereby increase the bioavailability of the micronutrient Fe. However, several studies have demonstrated that siderophore chelation may also *reduce* metal uptake by bacteria, fungi and plants and hence, siderophores may play a vital role in natural heavy metal detoxification (Braud et al., 2010; Höfte et al., 1993; O'Brien et al., 2014; Teitzel et al., 2006).

Siderophores are ubiquitous in almost all natural environments where organisms produce siderophores as a response to nutrient limitation (Kraemer et al., 2014). Concentrations in seawater are rather low (in the nanomolar range), whereas the highest concentrations are usually found in soils or soil solutions with concentrations up to the millimolar range (Kraemer, 2004; Watteau and Berthelin, 1994). The hydroxamate siderophore used in our study, desferrioxamine B (DFOB), is one of the most abundant and best-studied siderophores. In the modern environment, the biomolecule occurs in many soils (Winkelmann, 1992) and natural waters (Gledhill et al., 2004; McCormack et al., 2003). Besides a high affinity for binding Fe(III), DFOB is also very effective in binding with a range of other highly charged cations. DFOB readily binds and forms strong complexes with, for example, the rare earth elements and yttrium (REY), Mo, V, the platinum group elements and a range of actinides (e.g., Bau et al., 2013; Bouby *et al.*, 1998; Brantley *et al.*, 2001; Christenson and Schijf, 2011; Dahlheimer *et al.*, 2007; Hernlem *et al.*, 1996, 1999; Hussien *et al.*, 2013; Kraemer *et al.*, 2015a, 2015b, 2017; Liermann *et al.*, 2011; Mullen *et al.*, 2007; Ohnuki and Yoshida, 2012). Enhanced mobilization of Cr and Cr isotope fractionation from artificial Cr(III)-Fe(III)-(oxy)hydroxides in the presence of DFOB and oxalic acid was observed and attributed to two different processes: ligand-promoted solubilization and incongruent dissolution of the starting solid phases during water-mineral interaction (Saad et al., 2017a). Stewart et al. (2016) studied the desorptive release of Fe(III) and Cr(III) from goethite by DFOB. Using batch leaching experiments these authors showed that Cr(III) mobilization is significantly increased in the

presence of DFOB compared to ligand-free systems, although Cr(III) mobilization was by a factor of 60 lower than Fe(III) mobilization from goethite (Stewart et al., 2016).

Terrestrial cyanobacteria probably have produced organic compounds to accommodate nutrient deficiencies and heavy metal poisoning since at least 2.6 billion years (Liermann et al., 2005; Watanabe et al., 2000). Hence, the impact of organic ligands such as siderophores on trace metal cycling in the critical zone may have been significant since the late Neoarchean.

Organic ligands such as siderophores are capable of altering the trace element signal of igneous rocks during weathering and also of chemical sediments during their deposition (Bau et al., 2013; Kraemer et al., 2017, 2015b; Neaman, 2005). Duckworth et al. (2014) and Stewart et al. (2016) demonstrated that siderophores readily bind Cr and that the stability of Cr(III) complexes with DFOB are comparable to those of Fe(III)-DFOB complexes. Saad et al. (2017a) indicated that Cr(III)-(oxy)hydroxide solids may be resolubilized in subsurface environments due to the presence of microbial exudates such as siderophores. In this article we summarize the results of leaching experiments with DFOB conducted on different Cr-bearing igneous rocks and demonstrate the potential impact of DFOB on Cr mobility and Cr isotope fractionation in the environment.

2. Methods

2.1 Samples and experiments

2.1.1 Rock samples

We chose a range of igneous rocks and minerals for leaching experiments (described in 2.2) in order to assess whether the amount of Cr present and the rock type itself exert controls on siderophore-promoted Cr mobilization and/or may induce Cr isotope fractionation. Detailed information on the studied samples, their bulk rock Cr concentrations and δ^{53}Cr isotope values are provided in Table 1. For convenience, the samples are grouped into two distinct groups, namely *Group I: Silicate Rocks* and *Group II: Oxide Rocks*.

Group I: Silicate Rocks consists of the certified reference material *BHVO-2*, a Hawaiian basalt standard issued by the United States Geological Survey and the ocean island basalt *OIB-Me*. This is a primitive alkali basalt from Mehetia Island, Polynesia, and

described as sample Me90-05 in Binard et al. (1993). The core stone sample *CSAF3* is an Archean dolerite collected near Piet Retief, South Africa, and the komatiite samples Kom1 and Kom2 originate from the Pioneer Creek Formation in the Barberton Greenstone Belt, South Africa. The pyroxenite *PYRX* is a Cr-rich, platiniferous ultramafic rock from the Platreef Formation, Bushveld Igneous Complex, South Africa.

Group II: Oxide Rocks consists of *Taberg_1* and *Taberg_2* which are (titano)magnetites from Taberg volcano, Småland, Sweden, and of a magnetite from the magnetite-apatite deposit at Kiruna, Sweden (sample *Kiruna*). The magnetite samples *Mag_1a* and *Mag_1b* originate from the upper main magnetite layer of the Bushveld Complex in South Africa. The group further comprises chromitites from mafic/ultramafic layered intrusions in Southern Africa. Sample *GDCHR1* is a chromitite ore from the Great Dyke Igneous Complex, Zimbabwe, and samples *CHR1*, *BVCHR1* and *BVCHR2* are chromitites from the Eastern Bushveld Complex in South Africa.

Except for the spheroidally weathered dolerite, none of the samples are visibly altered. The crushed samples were rinsed with deionized water, dried and powdered to <63 µm with a Fritsch Pulverisette-6 planetary mill with agate balls and a sealed agate mortar in order to minimize sample contamination. Fine-milling does not represent natural conditions, but in order to demonstrate the principle viability of our hypothesis and to see whether or not siderophores exert any influence on Cr mobility and isotope fractionation, we decided to run the experiments with homogeneously fine-milled material. Bulk decompositions of the powdered rock samples were carried out using a DAS acid digestion system (Picotrace, Germany) following the mixed $HF/HClO_4$ acid digestion protocol outlined by Dulski (2001).

2.1.2 Leaching experiments

In this study, the DFOB siderophore was used to assess the impact of siderophores on Cr isotope fractionation. It is the best-studied siderophore to date and easily available in its mesylate form as the drug *Desferal*® (Novartis AG) which is commonly used to treat acute and chronic iron overload (Bernhardt, 2007; Nick et al., 2003). The leaching protocol was adapted from Kraemer et al. (2015b).

All batch leaching experiments were conducted in a trace-metal clean environment with acid-cleaned labware. Aliquots of exactly 1g of the dried and powdered rock samples were weighed out into acid-cleaned LDPE (low density polyethylene) bottles. The siderophore solutions were prepared separately with *Desferal*® and deionized water (DIW). The purity of *Desferal*® was checked by reagent blank measurements. The trace-element concentrations in pure *Desferal*® were found to be at least two orders of magnitude lower than the concentrations retrieved in the experiments. Solutions with 1mM and 10mM DFOB were prepared and its pH protocolled. The exact amount of siderophore solution matching a 20 g/l solid content was added to the reaction vessels containing the pre-weighed sample powders. These bottles were handshaken for a minute to facilitate dispersion and then placed on a shaker table set at 180 rpm. After 24 hours, the samples were removed from the shaker table and the solution was filtered using an acid-cleaned filter tower with a 0.2µm cellulose acetate membrane filter (both from Sartorius). The reaction vessels were not aired during the leaching experiments and the experiments were run in the dark in order to avoid the unlikely decomposition of organic matter by UV radiation and to avoid Cr photooxidation (e.g., Dai et al., 2010). The leachates were measured for pH and were then acidified with supra-pure hydrochloric acid to pH <2 and stored for later analysis of Cr isotopes (see 2.2) and for REY analysis using a low-resolution quadrupole ICP-MS Perkin-Elmer NexION 300.

Some experiments were carried out as replicates in order to demonstrate the overall reproducibility of the experimental approach and the analyses. The DFOB experiments on the magnetite Mag1a and on the chromitites GDCHR1, CHR1 and BVCHR2 were carried out twice, those with BVCHR1 three times. The general reproducibility is good with a maximum standard deviation of +0.054 ‰ units from the mean of the replicates. When Cr isotope determination in the siderophore solutions was impossible due to very low concentrations of dissolved Cr, the experiments were repeated at higher DFOB concentration of 10mM. In order to check whether simple organic acids may produce different effects, we also conducted experiments with 10mM citric acid (p.a. grade; PanReac AppliChem) instead of DFOB on representative samples from each of the two sample groups. Citric acid is an extracellular exudate and occurs at µM concentrations as a common constituent of many root and soil systems (e.g., Jones,

1998; Rovira, 1969). Control experiments were also conducted with deionized water without any organic ligands or acids. We emphasize, however, that in the absence of organic ligands, Cr is immobile and the Cr concentrations in the leachates are, therefore, much too low for the determination of $\delta^{53}Cr$ values for these control experiments. Chromium concentrations in the DI leachates were below the detection limit of the mass spectrometer (ca. 40 ng kg^{-1}).

2.2 Element and Isotope Analysis

2.2.1 Chromium concentrations and isotopes

Specific volumes of the different leaching solutions were spiked with an adequate amount of a ^{50}Cr-^{54}Cr double spike in 60ml Savillex vials before evaporation in a Teflon-coated carbon block on a hotplate at 100°C. The addition of a double spike enables correction of shifts in isotope abundances that might occur during the chemical purification and mass spectrometric analyses of the samples. Our Cr(III) ^{50}Cr-^{54}Cr double spike is characterized by the following fractional abundances: ^{50}Cr = 0.537971, ^{52}Cr = 0.035057, ^{53}Cr = 0.010869, and ^{54}Cr = 0.416103. We aimed for a Cr_{sample}/Cr_{spike} wgt-ratio of approximately 3:1. The dried samples were treated with approximately 1-2 ml of concentrated *aqua regia* to ensure spike-sample homogenization and dissolution of organic compounds and evaporated again. The samples were then subjected to a three-step Cr purification chromatography to isolate Cr from matrix elements. The dry samples were first redissolved in 1 ml of 6 mol l^{-1} HCl and poured onto 2 ml bed volume Poly-Prep® chromatographic columns packed with 1.5 ml of DOWEX AG-1 × 8 anion exchange resin (Bio-Rad Laboratories, 100–200 mesh) which retains Fe and allows Cr(III) to pass through. The Cr-containing solution was dried and subsequently re-dissolved in 25 ml of ultrapure water (Milli-Q system) doped with 2-3 drops of concentrated HCl to which 1 ml of a 0.1 mol l^{-1} $(NH_4)_2S_2O_8$ solution (Sigma-Aldrich, BioXra, N98%, St. Louis, MO, USA) was added. This step enables oxidation of Cr(III) to Cr(VI). The 60ml Savillex beakers were sealed and placed into a microwave oven and the solutions were boiled for 1 hour using the lowest (i.e. 90W) energy level to ensure complete oxidation of Cr. After cooling to room temperature, the Cr(VI) containing

247 solutions were passed over the pre-cleaned and re-conditioned 2 ml bed volume Poly-
248 Prep® chromatographic columns packed with 1.5 ml of DOWEX AG-1 × 8 anion
249 exchange resin (Bio-Rad Laboratories, 100–200 mesh) used for the respective Fe-clean-
250 ups. In these acidic solutions, Cr(VI)-oxyanions stick to the resin, while most other
251 elements (e.g. those with interfering isobaric Cr masses such as V and Ti) form cationic
252 or neutral complexes and are not adsorbed (Bonnand et al., 2011; Frei et al., 2012;
253 Schoenberg et al., 2008). Separation of the matrix elements and the elution of Cr
254 followed the purification procedure described by Schoenberg et al. (2008), with a few
255 modifications. As one of the modification, matrix elements were eluted from anion resin
256 using 10 ml of 0.1 mol l^{-1} HCl followed by 2 ml of 2 mol l^{-1} HCl. Cr was then eluted
257 following reduction and collected into 12 ml Savillex™ Teflon beakers with 8 ml of 2 mol
258 l^{-1} HNO_3, doped with 7 drops of 5% H_2O_2. The samples were subsequently evaporated
259 on a hot plate. The dried samples were re-dissolved in 100 µl of 12 mol l^{-1} HCl and
260 placed for 5 minutes on a hot plate to ensure complete dissolution. Subsequently, they
261 were taken up in 2.5 ml of ultrapure water and loaded on polypropylene chromatographic
262 columns (Evergreen Scientific) packed with 2ml of 200–400 mesh DOWEX AG 50W x 8
263 cation exchange resin (Bio-Rad Laboratories), which was preconditioned with 0.5 mol l^{-1}
264 HCl. This step separates Cr from matrix cations, such as Ca, K, Mg, Na and Mn. The
265 samples were immediately collected in the same 12 ml Savillex™ Teflon beakers. An
266 additional 8 ml of 0.5 mol l^{-1} HCl was added to elute the remaining Cr(III) from the resin.
267 Finally, the samples were evaporated to dryness. The cation exchange procedure was
268 adapted from Bonnand et al. (2011) and slightly modified. The procedural Cr yield is
269 approximately 60-70%. These yields compare to those reported by other authors
270 (Bonnand et al., 2011; Trinquier et al., 2008) for comparative procedures. These relatively
271 low yields do not affect the Cr isotope compositions, as we use a double spike for this
272 study. After drying down, the samples were loaded onto Re filaments in a mixture of 1.5
273 µl silica gel, 0.5 µl of 0.5 mol l^{-1} H_3PO_4, and 0.5 µl of 0.5 mol l^{-1} H_3BO_3 as described in
274 Frei et al. (2009). The samples were analyzed with an IsotopX PHOENIX thermal
275 ionization mass spectrometer (TIMS) at the University of Copenhagen, Denmark. The
276 mass spectrometer is equipped with eight Faraday collectors, allowing for simultaneous
277 monitoring of $^{50}Cr^{+}$, $^{52}Cr^{+}$, $^{53}Cr^{+}$, $^{54}Cr^{+}$, and of $^{49}Ti^{+}$, $^{51}V^{+}$, and $^{56}Fe^{+}$ which allows for

isobaric interference corrections of respective Cr masses $^{50}Cr^{+}$ and $^{54}Cr^{+}$ from Ti, V and Fe, respectively.

In the present work, we will use the established δ^{53}Cr notation which expresses the per mil deviation from standard reference material NIST SRM-979, calculated as:

Eq. 1: $$\delta^{53}\mathrm{Cr} = \left[\frac{\left(\frac{^{53}Cr}{^{52}Cr}\right)_{\text{sample}}}{\left(\frac{^{53}Cr}{^{52}Cr}\right)_{\text{SRM-979}}} - 1\right] x\ 1000\ ‰$$

Repeated analyses (N>200 analyses) of unprocessed double spiked SRM 979 standard samples yield Cr-isotope values that are slightly offset from the 0‰ value assigned to this standard. We measure δ^{53}Cr = 0.04±0.06‰ higher on the Phoenix (^{52}Cr = 500 mV) relative to the 0‰ certified SRM 979 value. The measured δ^{53}Cr values of our samples were corrected for this minimal offset.

The δ^{53}Cr notation uses the deviation from a standard material. In order to assess Cr isotope fractionation from bulk rock during leaching, we also employed a Δ^{53}Cr notation, which is defined as:

Eq. 2: $$\Delta^{53}\mathrm{Cr} = \delta^{53}Cr_{leach} - \delta^{53}Cr_{bulk}$$

2.2.2 Rare earth elements and yttrium

The leachates and bulk rock samples were analysed for rare earth elements and yttrium (REY) with a Perkin-Elmer NexION 300 quadrupole ICP-MS at Jacobs University Bremen, Germany. Ruthenium, Re, Rh and Bi served as internal standard elements to account for instrument drift and matrix effects and the certified reference material BHVO-2 (Basalt; United States Geological Survey) was used for quality control of the REY analysis. Background intensities of procedural blanks (acid digestion, DFOB solution, citric acid solution) were at least two orders of magnitude lower than sample intensities for the studied elements. Deviation from published literature values of sample BHVO-2 was <5% for all reported analytes.

3. Results

3.1 Bulk rock Cr concentrations and $\delta^{53}Cr_{bulk}$

Chromium concentrations in the bulk samples of *Group I: Silicate rocks* are between 55.42 mg kg^{-1} and 286 mg kg^{-1} and fall between 0.28 mg kg^{-1} to 34.1 wt.-% for those of *Group II: Oxide Rocks* (Table 1). Most bulk rock samples investigated in this study plot within the very narrow $\delta^{53}Cr_{bulk}$ range defined by Schoenberg et al. (2008) for high-temperature Cr (i.e., magmatic Cr, $\delta^{53}Cr$ = -0.124‰ to +0.101 ‰; Fig. 1). Hence, Cr isotopes of the bulk rocks mostly resemble those of primary magmatic rocks.

3.2 Chromium concentrations, $\delta^{53}Cr_{leach}$, $\Delta^{53}Cr$ of leachates

3.2.1 DFOB leachates

The pH of the DFOB leaching solution was 5.5 before the start of the experiments and went as high as 9.8 after 24 hours of leaching (Table 2). Leaching of different rock materials lead to different pH values of the solutions after leaching. The pH rose to a circumneutral value of about 7 to 8 in most experiments. The highest values with pH >8 were obtained during the komatiite, Taberg and Kiruna DFOB experiments.

Group I: Silicate rocks: Leaching of samples from this group in the presence of DFOB lead to mobilization of Cr from all investigated samples (Table 2). After 24 h incubation time, dissolved Cr concentrations in the leachates (measured solution concentrations; Table 2) were in the range of 1.3 µg kg^{-1} (BHVO-2) to 95 µg kg^{-1} (Kom2). The leachate of the weathered dolerite CSAF3 was significantly enriched in ^{53}Cr relative to ^{52}Cr and shows a positive $\delta^{53}Cr_{leach}$ value of +0.48 ± 0.07‰ and a positive $\Delta^{53}Cr$ value with +0.53‰. The DFOB leachates of the komatiites and pyroxenite show $\delta^{53}Cr_{leach}$ values in the range of -0.16 ± 0.086 to -0.05 ± 0.06‰ and negative $\Delta^{53}Cr$ values. Cr isotopes could not be quantified in leachates of basalts BHVO-2 and OIB-Me, due to very low Cr leachate concentrations, independent of the DFOB concentration used.

Group II: Oxide rocks: Cr was mobilized to different extents from all of these samples. Leachate concentrations from experiments with Taberg, Bushveld and Kiruna samples range from 1.3 µg kg^{-1} to 9.5 µg kg^{-1} Cr. However, Cr isotopes could only be determined for one leachate of the Taberg_1 titanomagnetite. This leachate shows the lightest $\delta^{53}Cr_{leach}$ value of -0.071 ± 0.09‰ of all analysed leachates. $\Delta^{53}Cr$ is positive (+0.079‰), but overlaps with bulk rock composition if the error is considered (± 0.09 ‰). Here, DFOB leaching apparently produced a solution that is isotopically similar to the bulk

source rock. Unfortunately, this is the only non-chromitite sample of *Group II: Oxide Rocks* for which Cr isotope measurement was possible even though the Taberg_2 sample was also treated with 10mM DFOB.

DFOB leachates of the chromitites are significantly enriched in Cr relative to the other Group II experiments with concentrations of 6.5 µg kg^{-1} *(BVCHR2)* to 108 µg kg^{-1} *(CHR1)*. The siderophore leachates of the chromitites are enriched in ^{53}Cr relative to ^{52}Cr and show positive $\delta^{53}Cr_{leach}$ values in the range of +0.15‰ ± 0.087‰ to +2.14‰ ± 0.042‰. Their $\Delta^{53}Cr$ values range from +0.11‰ to +2.19‰.

3.2.2 Citric acid leachates

The leachates of the citric acid experiments conducted with OIB-Me, CHR1 and GDCHR1 are enriched in Cr relative to the DFOB leachates, with concentrations ranging from 0.075 µg kg^{-1} to 1.39 mg kg^{-1}. However, the citric acid leachates are similar in their isotopic compositions relative to the respective bulk rocks, with $\delta^{53}Cr_{leach}$ values ranging from -0.11‰ ± 0.07‰ to -0.3‰ ± 0.10‰. Our results suggest that even a comparatively low concentration of citric acid mobilizes significant amounts of Cr from natural rock samples, but leaching in the presence of citric acid does *not* produce a significant Cr isotope fractionation. In comparison, DFOB leaching shows a stronger tendency toward ^{53}Cr mobilization (see Fig. 1).

3.3 Rare earth elements

Kraemer et al. (2015b, 2017) indicated that decoupling of the redox-sensitive lanthanide Ce from its strictly trivalent rare earth element neighbours La, Pr and Nd is observed when pristine igneous rocks are leached in the presence of DFOB. This decoupling is attributed to the oxidation of Ce(III) to Ce(IV) upon leaching in the presence of DFOB (Kraemer et al., 2015, 2017) and was referred to as the “siderophore redox pump”. As heavy Cr isotope fractionation is commonly observed when Cr(III) is oxidized to Cr(VI), we compared our Cr isotope findings to the REY distribution in the leachates. Bulk rock-normalized rare earth element and Y (REY_{BN}) data of the leachates from the present study are shown in Fig. 2 and leachate concentrations are reported in Table 3. REY determination was only possible on DFOB leachates of samples Taberg_1, Taberg_2,

OIB-Me, BHVO-2, Kiruna and GDCHR1. Unfortunately, REY concentrations in the chromitite leachates, except for GDCHR1, were below the detection limit of the utilized mass spectrometer due to very low REY abundances in the chromitite rocks and hence low concentrations in the leachates. Total REY concentrations in the leachates are in the range of 202 ng $kg^{-1}$to 21.067 ng kg^{-1} (Table 3). In order to demonstrate REY fractionation caused by the siderophore DFOB, the concentrations were normalized to bulk rock data (Fig. 2). The REY_{BN} patterns exhibit a distinct *positive* Ce_{BN} anomaly in *all* leachates and a depletion of light REY_{BN} relative to middle REY_{BN} and a concave downward pattern between La_{BN} and Sm_{BN}.

4. Discussion

4.1 Chromium mobilization and isotope fractionation in presence of the siderophore DFOB

The Cr concentrations in all DFOB leachates are similar within one to two orders of magnitude despite the fact that chromitites have up to several orders of magnitude higher Cr concentrations than many of the investigated silicate rocks (see Table 1). This suggests that the ligand concentration is the limiting factor for Cr release and not the amount of Cr in the rocks that is available for binding. The highest Cr concentrations in leachates were obtained in the CHR1-DFOB experiments and in the Kom2-DFOB experiments. However, the fractionation of Cr isotopes is markedly different between both experiments, with positive isotope fractionation and positive $\Delta^{53}Cr$ fractionation in the former and no fractionation and only very minor $\Delta^{53}Cr$ in the latter. Hence, neither the Cr concentration in the bulk rock nor the amount of Cr solubilized during leaching control Cr isotope fractionation in presence of siderophores.

Siderophore-promoted dissolution of silicate minerals has been demonstrated by, for example, Buss et al. (2007) and Liermann et al. (2005). These studies showed that siderophores are very efficient in dissolving silicate minerals, although dissolution proceeds at a lower rate than that of oxides. This is corroborated by the smaller amount of Cr mobilized from most pristine silicate rocks compared to chromitites observed in this study.

399 Fractionation of Cr isotopes from bulk rock values during leaching in the presence
400 of DFOB appears to some extent be limited to rocks in which Cr is bound to oxide or
401 hydroxide minerals. No significant isotope fractionation was observed during leaching of
402 pristine silicate rocks. As all experiments were conducted under the same (atmospheric)
403 conditions, oxygen fugacity can be ruled out as a significant control on DFOB-promoted
404 Cr isotope fractionation. Therefore, other mechanisms must exist that induce Cr stable
405 isotope fractionation during leaching from "oxide" rocks, but which do not cause
406 fractionation when pristine silicate rocks are leached. From the group of silicate rocks, the
407 strongly altered dolerite is the only one that produced a ^{53}Cr-enriched solution after it was
408 leached with DFOB. We suggest that the observed heavy isotope fractionation is related
409 to the presence of secondary mineral phases. Upon weathering, parts of the original
410 mineral assemblage in a pristine rock are decomposed due to chemical, physical and
411 biological processes. Olivine and pyroxene are among the first minerals to decompose
412 during oxidative weathering (Goldich, 1938) and secondary minerals form, which are
413 mostly clay minerals as well as (hydr)oxide minerals. High field-strength elements, i.e.
414 trace metals with high ionic potentials liberated during weathering, are bound to these
415 minerals due to sorption. As indicated above, siderophores are highly efficient in the
416 dissolution of (hydr)oxide minerals (Akafia et al., 2014; Kraemer, 2004; Saad et al.,
417 2017a). Present-day weathering occurs under oxidized conditions and secondary
418 minerals could be enriched in ^{53}Cr due to Cr redox reactions associated with oxidative
419 weathering and Cr fixation in secondary minerals. Hence, a preferred dissolution of these
420 secondary (hydr)oxides and a resolubilization of Cr by DFOB may explain the heavy Cr
421 isotope fractionation in the dolerite experiment.
422 Interaction of siderophores with Cr has been studied by, for example, Duckworth
423 et al. (2014) and Stewart et al. (2016). They indicated that complexes of Cr(III) with DFOB
424 have stabilities close to those of Fe(III) and estimated stability constants of around log K_f
425 = 30. Stability constants of metals with the hydroxamate siderophore DFOB (Hernlem et
426 al., 1996) and with the carboxylate siderophore rhizoferrin (Duckworth et al., 2014)
427 increase with increasing ionic potential of the complexed metal. Therefore, the oxidized
428 form of a metal has significantly higher stability constants with those two siderophores
429 than its reduced form. Reasoning from this observation, Kraemer et al. (2015b)

suggested an oxidative mobilization in the presence of DFOB for the redox-sensitive heavy metals Ce and U, a mechanism referred to as the "*siderophore-redox pump"* (Bau et al., 2013; Kraemer et al., 2015b). It is still unclear whether the DFOB siderophore actively or passively facilitates the oxidation of these redox-sensitive trace metals upon complexation.

Desferrixoamine B is also able to directly oxidize Fe(II) to Fe(III), also under strictly anaerobic conditions (Farkas et al., 2003, 2001). At least one of its hydroxamate functional groups is herein reduced to an amide (Eq. 3; Farkas et al., 2001; 2003).

Eq. 3: $2Fe^{2+} + 3H_4DFOB^{+} = 2[Fe(HDFOB)]^{+} + H_3DFOBmonoamide^{+} + H_20 + 4H^{+}$

(Farkas et al., 2001)

Oxidation of trivalent Ce to Ce(IV) was also suggested during mobilization of REY, during fluid-rock interaction, or during precipitation of chemical sediments in the presence of DFOB (Bau et al., 2013; Kraemer et al., 2017, 2015b). DFOB is a hydroxamate siderophore which contains three hydroxamate functional groups and past studies indicated that hydroxamate acids are also able to oxidize other redox-sensitive elements like Mo and V (Brown et al., 1996), Rh (Das et al., 2002) and U (Smith and Raymond, 1979).

All DFOB leachates produced in the study presented here exhibit positive Ce_{BN} anomalies (Fig. 2), regardless of whether oxide or (pristine) silicate rocks were leached. It is evident from Fig. 2 that all leachates for which REY concentrations could be determined, show decoupling of redox-sensitive Ce from its non-redox-sensitive, strictly trivalent REY neighbours. This supports previous results for igneous and pyroclastic material (Bau et al., 2013; Kraemer et al., 2015b). Such a decoupling of Ce from its REE neighbours can only be explained by the formation of Ce(IV) species in solution during leaching in presence of DFOB. If trivalent, Ce would, without exception, behave similar to its strictly trivalent REE neighbours La and Pr, also in presence of siderophores. If Ce(III)-DFOB complexes dominated the redox-speciation of Ce in solution, the corresponding REY_{BN} leachate pattern would be flat between La_{BN} and Pr_{BN} and no Ce_{BN} anomaly could have developed. This is incompatible with what is observed in our experiments (Fig. 2). A

striking question is why Ce is oxidized in *all* such experiments, while Cr stable isotope fractionation is limited to leaching of some oxide rocks and weathered silicate rocks. It may be assumed that in analogy to Ce, trivalent Cr is oxidized to Cr(VI) upon siderophore-rock interaction, similar to the oxidation observed during Fe- and Ce-DFOB interaction. However, using x-ray absorption spectroscopy (XAS), Cr(III)-DFOB complexes were shown to form upon leaching of $Cr(III)(OH)_3$ in presence of DFOB (Duckworth et al., 2014). This suggests that DFOB does not promote oxidation of Cr(III) upon solubilisation and ligand-binding. Additionally, the dominant aqueous Cr(VI) species is $Cr(VI)O_4^{2-}$, which results in a different siderophore binding mechanism compared to Ce(IV) and Fe(III), where Ce(IV)- and Fe(III)-DFOB complexes may form rather easily (see e.g., Kraemer et al., 2014; Ozaki et al., 2006). Therefore, other, non-redox-related mechanisms may be responsible for the observed stable isotope fractionation.

Redox-independent isotope fractionation in presence of DFOB was described for Fe (Brantley et al., 2004, 2001; Dideriksen et al., 2008; Morgan et al., 2010) and for Cu (Ryan et al., 2014). A study by Saad et al. (2017b) showed that siderophore and organic acid leaching of artificial Cr(III)-(oxy)hydroxide solids leads to isotope fractionation of dissolved Cr in the range of $\delta^{53}Cr$=+1.23 to -0.27 ‰, which is similar to the fractionation range observed in all our leachates. Redox-independent isotope fractionation may occur by one or a combination of several of the following mechanisms:

(a) Non-redox related Cr isotope fractionation may be caused by kinetic fractionation effects (Babechuk et al., 2018). Here, lighter isotopes are preferentially released from mineral surfaces, but the fractionation is a function of the size of the reactive surface sites and occurs only in the initial stages of a dissolution process (Wiederhold et al., 2006). However, light isotope enrichment was not observed in our experiments with DFOB and citric acid.

(b) Stable isotope fractionation during leaching may also occur due to incongruent dissolution of polymineralic rocks comprised of minerals that show different isotope ratios. This was shown for Fe (Chapman et al., 2009) and Mo (Voegelin et al., 2010) and recently also for Cr isotopes by Novak et al. (2017), who report a certain $\delta^{53}Cr$ isotope fractionation due to incongruent weathering of ultramafic rocks.

(c) Equilibrium stable isotope fractionation may occur due to different bonding environments between the metal-ligand complex in solution and metal-ligand complexes sorbed to the mineral surface (Wiederhold, 2015). Strong binding ligands, i.e. ligands with high stability constants with the complexed metal, may cause enrichment of heavy isotopes in solution (Criss, 1999). According to Saad et al. (2017a), equilibrium stable isotope fractionation in combination with incongruent dissolution of the starting material lead to the observed Cr isotope fractionation during leaching of artificial Cr(III)-bearing oxyhydroxides. The enrichment of heavy Cr isotopes in solution, therefore, is then caused by the stronger Cr(III)-oxygen bonds in the ligand compared to the Cr(III)-oxygen bonds in the solid (Saad et al., 2017b).

In our experiments, equilibrium stable isotope fractionation must have controlled the isotope fractionation to some extent simply due to the very high complex stability constants of the DFOB siderophore with Cr in the range of log k_f = 30 (Duckworth et al., 2014). The different trends in isotope fractionation in the DFOB experiments, however, cannot solely be explained by this process. In most natural rock samples, Cr is polymodally distributed as a trace element over several mineral phases. Novak et al. (2017) present δ^{53}Cr of whole rocks as well as mineral separates of serpentinite and (altered) peridotites and show that especially the minerals chlorite, hornblende and albite are enriched in ^{53}Cr relative to ^{52}Cr. Serpentinite mineral separates, on the other hand, yield δ^{53}Cr isotope variations in the range of -0.29 to +0.4 (Novak et al., 2017). Therefore, each mineral phase in a natural rock sample may have a markedly different Cr isotope composition. The chromitites studied here are mainly composed of (Mg-)chromite (>95%) and to lesser extents olivine, pyroxene and anorthitic feldspar. As δ^{53}Cr of the bulk rock is unfractionated relative to bulk Earth, we assume that the mineral chromite, which is the major constituent of chromitite, is also unfractionated in δ^{53}Cr relative to bulk Earth. However, the DFOB leachates of the chromitite rocks are significantly enriched in ^{53}Cr, indicating that either i) the mobilized Cr originates from a ^{53}Cr-enriched mineral phase (which is not chromite) and/or ii) that Cr was liberated from isotopically unfractionated chromite and the observed isotope fractionation is the result of equilibrium isotope fractionation.

521 The siderophore DFOB, therefore, may enhance Cr transport into solution and may
522 cause, depending on the rock type, Cr isotope fractionation. Citric acid, on the other
523 hand, leads to an elevated mobilization of Cr compared to DFOB, but the pH suggests
524 that proton-promoted dissolution is prevalent and the solutions are not fractionated in
525 their Cr isotope compositions relative to bulk rock $\delta^{53}Cr$ values. Our findings confirm the
526 experimental results of Saad et al. (2017b), which indicate lack of significant isotope
527 fractionation during leaching in presence of citric acid as well as in presence of other
528 organic acids.
529
530 **4.2 Implications for (paleo-)environmental studies**
531 The widespread use of Cr as an alloy and in electroplating, tanning and dyeing
532 introduces large amounts of Cr into the environment and, hence, Cr can become a
533 serious anthropogenic pollutant (Cervantes et al., 2001; Kotaś and Stasicka, 2000). In
534 terms of toxicity, Cr^{6+} is generally considered the most toxic redox-species because of the
535 production of free radicals in living cells during reduction of Cr^{6+} to lower oxidation states
536 (Cervantes et al., 2001; Kadiiska et al., 1994). However, Cr^{3+} can also be detrimental to
537 living cells, albeit at higher concentrations than Cr^{6+} and via a markedly different uptake
538 mechanism (Skeffington et al., 1976). Dissolved Cr levels of river water are on average
539 0.7 µg kg^{-1} (Gaillardet et al., 2013) and seawater Cr concentrations are 0.156 µg kg^{-1} in
540 the open ocean (Bruland and Lohan, 2004). However, river water can be highly enriched
541 in Cr if Cr-processing industries are located in the river catchment. For example, up to
542 1.46 µg kg^{-1} Cr were found in waters of the river Mouttas, Algeria, downstream of a large
543 tannery (Leghouchi et al., 2009). This highlights the need for efficient remediation
544 techniques to clean up ground and river waters and contaminated soils. Cervantes et al.
545 (2001) discuss bioremediation of Cr in detail. Bioremediation of Cr has only been
546 investigated at a lab-scale and is to date not done at a larger scale. The high affinity of
547 siderophores for Cr in general suggests that siderophores are, in principle, viable for the
548 remediation of Cr-contaminated soils and surface waters. Remediation of Cr-
549 contaminated sites usually involves a reduction of Cr(VI) to Cr(III), efficiently immobilizing
550 Cr. However, by means of immobilizing DFOB, e.g. via sorption to clay minerals (Maurice
551 et al., 2009), or by using siderophores for metal removal from contaminated soil as

indicated for other heavy metals (Frazier et al., 2005; Nair et al., 2007), remediation of Cr-contaminated sites might be feasible. This opens the venue for future, yet more detailed, studies. Some plants are able to hyperaccumulate Cr (Baker and Brooks, 1989) and the presence of organic ligands like oxalic acid and malate enhances the accumulation of Cr in plants (Srivastava et al., 1999). Siderophores may play a similar, yet more element-specific role in enhancing bioavailability due to their affinity towards highly-charged ions with small ionic radii (high ionic potential) and especially due to their affinity for redox-sensitive trace elements. However, this could not be observed in a most recent study of the potential role of siderophores during REE uptake by the bolete mushroom *Suillus luteus* (Zocher et al., 2018).

Chromium isotopes are also increasingly used as a paleo-redox proxy (Crowe et al., 2013; Frei et al., 2009; Planavsky et al., 2014; Gilleaudeau et al., 2016; Frei et al., 2016). Other redox-sensitive elements such as Ce and U (Bau and Alexander, 2009; Bau and Dulski, 1996; Kamber et al., 2014; Kendall et al., 2013; Nakada et al., 2016; Partin et al., 2013; Schier et al., 2018; Viehmann et al., 2016, 2015) or Mo (Anbar et al., 2007; Asael et al., 2013; Duan et al., 2010; Kurzweil et al., 2015; Voegelin et al., 2010) are also used as geochemical proxies to evaluate the evolution of the redox level of the Earth's surface environments throughout geological history. However, biogenic ligands were *probably* produced since at least the Mesoproterozoic (Neaman, 2005; Raven, 1995). Past studies on the interaction of DFOB with Mo reported enhanced Mo mobilization rates as well as an enrichment of heavy Mo isotopes in solutions containing DFOB (Liermann et al., 2005; Liermann et al., 2011). Hence, hydroxamate siderophores are also capable of facilitating stable isotope fractionation of other redox-sensitive elements like Mo and supposedly also V, also under strictly anaerobic conditions. As biogenic ligands, especially hydroxamate siderophores, may affect the mobilization and isotope fractionation of certain trace elements, the potential availability of siderophores in these past environments needs to be considered before redox-sensitive elements and their isotopes may be used as robust quantitative paleo-redox proxies. Siderophores and their unique capabilities in binding highly-charged metals may also have a huge potential for a better understanding of the geobiological evolution of Early Earth and the appearance of the earliest life on Earth and in our solar system.

5. Conclusion

The presence of the DFOB siderophore during leaching leads to mobilization of Cr(III) from igneous rock samples and stable Cr isotope fractionation. DFOB-enhanced mobilization is not limited to the redox-sensitive trace elements Ce and U (Kraemer et al., 2017, 2015b; Tanaka et al., 2010 and others), but also affects the redox-sensitive heavy transition metal Cr. Chromium isotopes are fractionated upon leaching with DFOB. These findings further improve the understanding of how redox proxies in modern and ancient environments work and how to evaluate the geochemical interpretation of redox-sensitive elements in geochemical archives. In modern oxidized environments, MnO_2 is responsible for Cr oxidation and the isotope fractionation associated with the oxidation process (Kotaś and Stasicka, 2000). In anoxic systems, however, H_2O_2 is able to promote Cr oxidation (Oze et al., 2016). Our findings indicate that the presence of specific organic ligands with a high affinity for Cr are also able to fractionate Cr isotopes, supposedly also under anoxic conditions. This supports the findings of Saad et al. (2017b) and expands the database on Cr-DFOB interaction to natural rock samples.

Stable isotope fractionation as well as the reported mobilization/fractionation of redox-sensitive elements like Ce, U, Mo, V, and W could therefore also act as "fingerprints" for the presence of biogenic compounds in rocks and soils and may thus serve as proxies for the presence of "life" in the sense of *biosignatures*. However, this definitely requires further research and any such statements made are premature unless the whole system is understood in detail.

References

Akafia, M.M., Harrington, J.M., Bargar, J.R., Duckworth, O.W., 2014. Metal Oxyhydroxide Dissolution as Promoted by Structurally Diverse Siderophores and Oxalate. Geochim. Cosmochim. Acta 141, 258–269. doi:10.1016/j.gca.2014.06.024

Arcy, J.D., Babechuk, M.G., Døssing, L.N., Frei, R., Gaucher, C., 2016. Processes controlling the chromium isotopic composition of river water : Constrains from basaltic river catchments. Geochim. Cosmochim. Acta. doi:10.1016/j.gca.2016.04.027

Babechuk, M.G., Kleinhanns, I.C., Reitter, E., Schoenberg, R., 2018. Kinetic stable Cr isotopic fractionation between aqueous Cr(III)-Cl-H 2 O complexes at 25 °C: implications for Cr(III) mobility and isotopic variations in modern and ancient natural

618 systems. Geochim. Cosmochim. Acta 222, 383–405. doi:10.1016/j.gca.2017.10.002
619 Babechuk, M.G., Kleinhanns, I.C., Schoenberg, R., 2017. Chromium geochemistry of the
620 ca. 1.85 Ga Flin Flon paleosol. Geobiology 15, 30–50. doi:10.1111/gbi.12203
621 Baker, A.J.M., Brooks, R.R., 1989. Terrestrial higher plants which hyperaccumulate
622 metallic elements - a review of their distribution, ecology and phytochemistry.
623 Biorecovery 1, 81–126.
624 Basu, A., Johnson, T.M., Sanford, R. a., 2014. Cr isotope fractionation factors for Cr(VI)
625 reduction by a metabolically diverse group of bacteria. Geochim. Cosmochim. Acta
626 142, 349–361. doi:10.1016/j.gca.2014.07.024
627 Bau, M., Alexander, B.W., 2009. Distribution of high field strength elements (Y, Zr, REE,
628 Hf, Ta, Th, U) in adjacent magnetite and chert bands and in reference standards
629 FeR-3 and FeR-4 from the Temagami iron-formation, Canada, and the redox level
630 of the Neoarchean ocean. Precambrian Res. 174, 337–346.
631 doi:10.1016/j.precamres.2009.08.007
632 Bau, M., Dulski, P., 1996. Distribution of yttrium and rare-earth elements in the Penge
633 and Kuruman iron-formations, Transvaal Supergroup, South Africa. Precambrian
634 Res. 79, 37–55.
635 Bau, M., Tepe, N., Mohwinkel, D., 2013. Siderophore-promoted transfer of rare earth
636 elements and iron from volcanic ash into glacial meltwater, river and ocean water.
637 Earth Planet. Sci. Lett. 364, 30–36. doi:10.1016/j.epsl.2013.01.002
638 Berna, E.C., Johnson, T.M., Makdisi, R.S., Basu, A., 2010. Cr Stable Isotopes As
639 Indicators of Cr(VI) Reduction in Groundwater: A Detailed Time-Series Study of a
640 Point-Source Plume. Environ. Sci. Technol. 44, 1043–1048. doi:10.1021/es902280s
641 Bernhardt, P. V, 2007. Coordination chemistry and biology of chelators for the treatment
642 of iron overload disorders. Dalton Trans. 3214–20. doi:10.1039/b708133b
643 Binard, N., Maury, R.C., Guille, G., Talandier, J., Gillot, P.Y., Cotten, J., 1993. Mehetia
644 Island, South Pacific: geology and petrology of the emerged part of the Society hot
645 spot. J. Volcanol. Geotherm. Res. 55, 239–260. doi:10.1016/0377-0273(93)90040-X
646 Bouby, M., Billard, I., MacCordick, J., 1998. Complexation of Th (IV) with the siderophore
647 pyoverdine A. J. Alloys Compd. 271–273, 206–210. doi:10.1016/S0925-
648 8388(98)00055-3
649 Brantley, S.L., Liermann, L., Bau, M., Wu, S., 2001. Uptake of Trace Metals and Rare
650 Earth Elements from Hornblende by a Soil Bacterium. Geomicrobiol. J. 18, 37–61.
651 doi:10.1080/01490450151079770
652 Brantley, S.L., Liermann, L.J., Guynn, R.L., Anbar, A., Icopini, G.A., Barling, J., 2004. Fe
653 isotopic fractionation during mineral dissolution with and without bacteria. Geochim.
654 Cosmochim. Acta 68, 3189–3204. doi:10.1016/j.gca.2004.01.023
655 Braud, A., Geoffroy, V., Hoegy, F., Mislin, G.L.A., Schalk, I.J., 2010. Presence of the
656 siderophores pyoverdine and pyochelin in the extracellular medium reduces toxic
657 metal accumulation in Pseudomonas aeruginosa and increases bacterial metal
658 tolerance. Environ. Microbiol. Rep. 2, 419–25. doi:10.1111/j.1758-
659 2229.2009.00126.x
660 Brown, D.A., Bögge, H., Coogan, R., Doocey, D., Kemp, T.J., Müller, A., Neumann, B.,
661 1996. Oxygen Abstraction Reactions of N-Substituted Hydroxamic Acids with
662 Molybdenum(V) and Vanadium(III) and -(IV) Compounds. Inorg. Chem. 35, 1674–
663 1679. doi:10.1021/ic950819r
664 Buss, H.L., Lüttge, A., Brantley, S.L., 2007. Etch pit formation on iron silicate surfaces
665 during siderophore-promoted dissolution. Chem. Geol. 240, 326–342.
666 doi:10.1016/j.chemgeo.2007.03.003
667 Canfield, D.E., Zhang, S., Frank, A.B., Wang, X., Wang, H., Su, J., Ye, Y., Frei, R., 2018.
668 Highly fractionated chromium isotopes in Mesoproterozoic-aged shales and
669 atmospheric oxygen. Nat. Commun. 9, 2871. doi:10.1038/s41467-018-05263-9
670 Cervantes, C., Campos-García, J., Devars, S., Gutiérrez-Corona, F., Loza-Tavera, H.,
671 Torres-Guzmán, J.C., Moreno-Sánchez, R., 2001. Interactions of chromium with

672 microorganisms and plants. FEMS Microbiol. Rev. 25, 335–347. doi:10.1111/j.1574-
673 6976.2001.tb00581.x

674 Chapman, J.B., Weiss, D.J., Shan, Y., Lemburger, M., 2009. Iron isotope fractionation
675 during leaching of granite and basalt by hydrochloric and oxalic acids. Geochim.
676 Cosmochim. Acta 73, 1312–1324. doi:10.1016/j.gca.2008.11.037

677 Christenson, E., Schijf, J., 2011. Stability of YREE complexes with the trihydroxamate
678 siderophore desferrioxamine B at seawater ionic strength. Geochim. Cosmochim.
679 Acta 75, 7047–7062. doi:10.1016/j.gca.2011.09.022

680 Cole, D.B., Reinhard, C.T., Wang, X., Gueguen, B., Halverson, G.P., Gibson, T.,
681 Hodgskiss, M.S.W., McKenzie, N.R., Lyons, T.W., Planavsky, N.J., 2016. A shale-
682 hosted Cr isotope record of low atmospheric oxygen during the Proterozoic.
683 Geology 44, 555–558. doi:10.1130/G37787.1

684 Criss, R.E., 1999. Principles of stable isotope distribution. Oxford University Press.

685 Crowe, S.A., Døssing, L.N., Beukes, N.J., Bau, M., Kruger, S.J., Frei, R., Canfield, D.E.,
686 2013. Atmospheric oxygenation three billion years ago. Nature 501, 535–8.
687 doi:10.1038/nature12426

688 Dahlheimer, S.R., Neal, C.R., Fein, J.B., 2007. Potential Mobilization of Platinum-Group
689 Elements by Siderophores in Surface Environments. Environ. Sci. Technol. 41,
690 870–875. doi:10.1021/es0614666

691 Dai, R., Yu, C., Liu, J., Lan, Y., Deng, B., 2010. Photo-Oxidation of Cr(III)−Citrate
692 Complexes Forms Harmful Cr(VI). Environ. Sci. Technol. 44, 6959–6964.
693 doi:10.1021/es100902y

694 Das, A., Basuli, F., Peng, S.-M., Bhattacharya, S., 2002. Oxidation of Rhodium(I) by
695 Hydroxamic Acids. Synthesis, Structure, and Electrochemical Properties of
696 Bis(hydroxamate) Complexes of Rhodium(III). Inorg. Chem. 41, 440–443.
697 doi:10.1021/ic0106930

698 Dideriksen, K., Baker, J.A., Stipp, S.L.S., 2008. Equilibrium Fe isotope fractionation
699 between inorganic aqueous Fe(III) and the siderophore complex, Fe(III)-
700 desferrioxamine B. Earth Planet. Sci. Lett. 269, 280–290.
701 doi:10.1016/j.epsl.2008.02.022

702 Duckworth, O.W., Akafia, M.M., Andrews, M.Y., Bargar, J.R., 2014. Siderophore-
703 promoted dissolution of chromium from hydroxide minerals. Environ. Sci. Process.
704 Impacts 16, 1348–1359. doi:10.1039/C3EM00717K

705 Dulski, P., 2001. Reference Materials for Geochemical Studies: New Analytical Data by
706 ICP-MS and Critical Discussion of Reference Values. Geostand. Geoanalytical Res.
707 25, 87–125. doi:10.1111/j.1751-908X.2001.tb00790.x

708 Economou-Eliopoulos, M., Frei, R., Atsarou, C., 2014. Application of chromium stable
709 isotopes to the evaluation of Cr(VI) contamination in groundwater and rock
710 leachates from central Euboea and the Assopos basin (Greece). Catena 122, 216–
711 228. doi:10.1016/j.catena.2014.06.013

712 Ellis, A.S., Johnson, T.M., Villalobos-Aragon, A., Bullen, T.D., 2008. Ellis AS, Johnson
713 TM, Villalobos-Aragon A, Bullen T (2008) Environmental cycling of Cr using stable
714 isotopes: kinetic and equilibrium effects, in: AGU Fall Meeting.

715 Farkas, E., Enyedy, É.., Fábián, I., 2003. New insight into the oxidation of Fe(II) by
716 desferrioxamine B (DFB): spectrophotometric and capillary electrophoresis (CE)
717 study. Inorg. Chem. Commun. 6, 131–134. doi:10.1016/S1387-7003(02)00703-7

718 Farkas, E., Enyedy, E.A., Zékány, L., Deák, G., 2001. Interaction between iron(II) and
719 hydroxamic acids: oxidation of iron(II) to iron(III) by desferrioxamine B under
720 anaerobic conditions. J. Inorg. Biochem. 83, 107–14.

721 Fendorf, S.E., 1995. Surface reactions of chromium in soils and waters. Geoderma 67,
722 55–71. doi:10.1016/0016-7061(94)00062-F

723 Frazier, S.W., Kretzschmar, R., Kraemer, S.M., 2005. Bacterial Siderophores Promote
724 Dissolution of UO 2 under Reducing Conditions. Environ. Sci. Technol. 39, 5709–
725 5715. doi:10.1021/es050270n

726 Frei, R., Crowe, S.A., Bau, M., Polat, A., Fowle, D.A., Døssing, L.N., 2016. Oxidative
727 elemental cycling under the low O2 Eoarchean atmosphere. Sci. Rep. 6:21058, 1–9.
728 doi:10.1038/srep21058

729 Frei, R., Gaucher, C., Poulton, S.W., Canfield, D.E., 2009. Fluctuations in Precambrian
730 atmospheric oxygenation recorded by chromium isotopes. Nature 461, 250–3.
731 doi:10.1038/nature08266

732 Frei, R., Rosing, M.T., 2005. Search for traces of the late heavy bombardment on Earth—
733 Results from high precision chromium isotopes. Earth Planet. Sci. Lett. 236, 28–40.
734 doi:10.1016/j.epsl.2005.05.024

735 Gilleaudeau, G.J., Frei, R., Kaufman, A.J., Kah, L.C., Azmy, K., Bartley, J.K.,
736 Chernyavskiy, P., Knoll, A.H., 2016. Oxygenation of the mid-Proterozoic
737 atmosphere: clues from chromium isotopes in carbonates. Geochemical Perspect.
738 Lett. 178–187. doi:10.7185/geochemlet.1618

739 Gledhill, M., McCormack, P., Ussher, S., Achterberg, E.P., Mantoura, R.F.C., Worsfold,
740 P.J., 2004. Production of siderophore type chelates by mixed bacterioplankton
741 populations in nutrient enriched seawater incubations. Mar. Chem. 88, 75–83.
742 doi:10.1016/j.marchem.2004.03.003

743 Han, R., Qin, L., Brown, S.T., Christensen, J.N., Beller, H.R., 2012. Differential isotopic
744 fractionation during Cr(VI) reduction by an aquifer-derived bacterium under aerobic
745 versus denitrifying conditions. Appl. Environ. Microbiol. 78, 2462–4.
746 doi:10.1128/AEM.07225-11

747 Hernlem, B.J., Vane, L.M., Sayles, G.D., 1999. The application of siderophores for metal
748 recovery and waste remediation: examination of correlations for prediction of metal
749 affinities. Water Res. 33, 951–960.

750 Hernlem, B.J., Vane, L.M., Sayles, G.D., 1996. Stability constants for complexes of the
751 siderophore desferrioxamine B with selected heavy metal cations. Inorganica Chim.
752 Acta 244, 179–184. doi:10.1016/0020-1693(95)04780-8

753 Höfte, M., Buysens, S., Koedam, N., Cornelis, P., 1993. Zinc affects siderophore-
754 mediated high affinity iron uptake systems in the rhizosphere Pseudomonas
755 aeruginosa 7NSK2. Biometals 6. doi:10.1007/BF00140108

756 Holmden, C., Jacobson, A.D., Sageman, B.B., Hurtgen, M.T., 2016. Response of the Cr
757 isotope proxy to Cretaceous Ocean Anoxic Event 2 in a pelagic carbonate
758 succession from the Western Interior Seaway. Geochim. Cosmochim. Acta 186,
759 277–295. doi:10.1016/J.GCA.2016.04.039

760 Huang, J., Liu, J., Zhang, Y., Chang, H., Shen, Y., Huang, F., Qin, L., 2018. Cr isotopic
761 composition of the Laobao cherts during the Ediacaran–Cambrian transition in
762 South China. Chem. Geol. 482, 121–130. doi:10.1016/J.CHEMGEO.2018.02.011

763 Hussien, S.S., Desouky, O.A., Abdel-Haliem, M.E.F., El-Mougith, A.A., 2013. Uranium
764 (VI) Complexation with Siderophores-pyoverdine Produced by Pseudomonas
765 Fluorescens SHA 281. Int. J. Nucl. Energy Sci. Eng. 3, 95.
766 doi:10.14355/ijnese.2013.0304.03

767 Izbicki, J.A., Bullen, T.D., Martin, P., Schroth, B., 2012. Delta Chromium-53/52 isotopic
768 composition of native and contaminated groundwater, Mojave Desert, USA. Appl.
769 Geochemistry 27, 841–853. doi:10.1016/J.APGEOCHEM.2011.12.019

770 Jones, D.L., 1998. Organic acids in the rhizosphere – a critical review. Plant Soil 205, 25–
771 44. doi:10.1023/A:1004356007312

772 Kamber, B.S., Webb, G.E., Gallagher, M., 2014. The rare earth element signal in
773 Archaean microbial carbonate: information on ocean redox and biogenicity. J. Geol.
774 Soc. London. 171, 745–763. doi:10.1144/jgs2013-110

775 Kendall, B., Brennecka, G.A., Weyer, S., Anbar, A.D., 2013. Uranium isotope
776 fractionation suggests oxidative uranium mobilization at 2.50Ga. Chem. Geol. 362,
777 105–114. doi:10.1016/j.chemgeo.2013.08.010

778 Kortenkamp, A., Casadevall, M., Faux, S.P., Jenner, A., Shayer, R.O.J., Woodbridge, N.,
779 O'Brien, P., 1996. A Role for Molecular Oxygen in the Formation of DNA Damage
780 during the Reduction of the Carcinogen Chromium(VI) by Glutathione. Arch.

781 Biochem. Biophys. 329, 199–207. doi:10.1006/abbi.1996.0209
782 Kotaś, J., Stasicka, Z., 2000. Chromium occurrence in the environment and methods of
783 its speciation. Environ. Pollut. 107, 263–283. doi:10.1016/S0269-7491(99)00168-2
784 Kraemer, D., Junge, M., Oberthür, T., Bau, M., 2015a. Improving Recoveries of Platinum
785 and Palladium from Oxidized Platinum-Group Element Ores of the Great Dyke,
786 Zimbabwe, using the biogenic Siderophore Desferrioxamine B. Hydrometallurgy
787 152, 169–177. doi:10.1016/j.hydromet.2015.01.002
788 Kraemer, D., Kopf, S., Bau, M., 2015b. Oxidative mobilization of cerium and uranium and
789 enhanced release of “immobile” high field strength elements from igneous rocks in
790 the presence of the biogenic siderophore desferrioxamine B. Geochim. Cosmochim.
791 Acta 165, 263–279. doi:10.1016/j.gca.2015.05.046
792 Kraemer, D., Tepe, N., Pourret, O., Bau, M., 2017. Negative cerium anomalies in
793 manganese (hydr)oxide precipitates due to cerium oxidation in the presence of
794 dissolved siderophores. Geochim. Cosmochim. Acta 196, 197–208.
795 doi:10.1016/j.gca.2016.09.018
796 Kraemer, S.M., 2004. Iron oxide dissolution and solubility in the presence of
797 siderophores. Aquat. Sci. Res. Across Boundaries 66, 3–18. doi:10.1007/s00027-
798 003-0690-5
799 Kraemer, S.M., Duckworth, O.W., Harrington, J.M., Schenkeveld, W.D.C., 2014.
800 Metallophores and Trace Metal Biogeochemistry. Aquat. Geochemistry 21, 159–
801 195. doi:10.1007/s10498-014-9246-7
802 Liermann, L.J., Guynn, R.L., Anbar, A., Brantley, S.L., 2005. Production of a
803 molybdophore during metal-targeted dissolution of silicates by soil bacteria. Chem.
804 Geol. 220, 285–302. doi:10.1016/j.chemgeo.2005.04.013
805 Liermann, L.J., Mathur, R., Wasylenki, L.E., Nuester, J., Anbar, A.D., Brantley, S.L.,
806 2011. Extent and isotopic composition of Fe and Mo release from two Pennsylvania
807 shales in the presence of organic ligands and bacteria. Chem. Geol. 281, 167–180.
808 doi:10.1016/j.chemgeo.2010.12.005
809 Lytle, C.M., Lytle, F.W., Yang, N., Qian, J.-H., Hansen, D., Zayed, A., Terry, N., 1998.
810 Reduction of Cr(VI) to Cr(III) by Wetland Plants: Potential for In Situ Heavy Metal
811 Detoxification. Environ. Sci. Technol. 32, 3087–3093. doi:10.1021/ES980089X
812 Maurice, P., Haack, E., Mishra, B., 2009. Siderophore sorption to clays. Biometals 22,
813 649–658. doi:10.1007/s10534-009-9242-3
814 McCormack, P., Worsfold, P.J., Gledhill, M., 2003. Separation and Detection of
815 Siderophores Produced by Marine Bacterioplankton Using High-Performance Liquid
816 Chromatography with Electrospray Ionization Mass Spectrometry. Anal. Chem. 75,
817 2647–2652. doi:10.1021/ac0340105
818 Morgan, J.L.L., Wasylenki, L.E., Nuester, J., Anbar, A.D., 2010. Fe Isotope Fractionation
819 during Equilibration of Fe−Organic Complexes. Environ. Sci. Technol. 44, 6095–
820 6101. doi:10.1021/es100906z
821 Mullen, L., Gong, C., Czerwinski, K., 2007. Complexation of uranium (VI) with the
822 siderophore desferrioxamine B. J. Radioanal. Nucl. Chem. 273, 683–688.
823 doi:10.1007/s10967-007-0931-5
824 Nair, A., Juwarkar, A.A., Singh, S.K., 2007. Production and Characterization of
825 Siderophores and its Application in Arsenic Removal from Contaminated Soil.
826 Water. Air. Soil Pollut. 180, 199–212. doi:10.1007/s11270-006-9263-2
827 Nakada, R., Takahashi, Y., Tanimizu, M., 2016. Cerium stable isotope ratios in
828 ferromanganese deposits and their potential as a paleo-redox proxy. Geochim.
829 Cosmochim. Acta 181, 89–100. doi:10.1016/j.gca.2016.02.025
830 Neaman, A., 2005. Implications of the evolution of organic acid moieties for basalt
831 weathering over geological time. Am. J. Sci. 305, 147–185.
832 doi:10.2475/ajs.305.2.147
833 Nick, H., Acklin, P., Lattmann, R., Buehlmayer, P., Hauffe, S., Schupp, J., Alberti, D.,
834 2003. Development of Tridentate Iron Chelators: From Desferrithiocin to ICL670.

835 Curr. Med. Chem. 10, 1065–1076. doi:10.2174/0929867033457610

836 Novak, M., Kram, P., Sebek, O., Andronikov, A., Chrastny, V., Martinkova, E., Stepanova,
837 M., Prechova, E., Curik, J., Veselovsky, F., Myska, O., Stedra, V., Farkas, J., 2017.
838 Temporal changes in Cr fluxes and δ 53 Cr values in runoff from a small
839 serpentinite catchment (Slavkov Forest, Czech Republic). Chem. Geol. 472, 22–30.
840 doi:10.1016/j.chemgeo.2017.09.023

841 O'Brien, S., Hodgson, D.J., Buckling, A., 2014. Social evolution of toxic metal
842 bioremediation in Pseudomonas aeruginosa. Proc. Biol. Sci. 281, 20140858-.
843 doi:10.1098/rspb.2014.0858

844 Ohnuki, T., Yoshida, T., 2012. Interactions of the Rare Earth Elements-Desferrioxamine B
845 Complexes with Pseudomonas fluorescens and y-Al2O3. Chem. Lett. 41, 98–100.
846 doi:http://dx.doi.org/10.1246/cl.2012.98

847 Owlad, M., Aroua, M.K., Daud, W.A.W., Baroutian, S., 2009. Removal of Hexavalent
848 Chromium-Contaminated Water and Wastewater: A Review. Water. Air. Soil Pollut.
849 200, 59–77. doi:10.1007/s11270-008-9893-7

850 Ozaki, T., Suzuki, Y., Nankawa, T., Yoshida, T., Ohnuki, T., Kimura, T., Francis, A.J.,
851 2006. Interactions of rare earth elements with bacteria and organic ligands. J. Alloys
852 Compd. 408–412, 1334–1338. doi:10.1016/j.jallcom.2005.04.142

853 Oze, C., Bird, D.K., Fendorf, S., 2007. Genesis of hexavalent chromium from natural
854 sources in soil and groundwater. Proc. Natl. Acad. Sci. U. S. A. 104, 6544–9.
855 doi:10.1073/pnas.0701085104

856 Oze, C., Sleep, N.H., Coleman, R.G., Fendorf, S., 2016. Anoxic oxidation of chromium.
857 Geology 44, 543–546. doi:10.1130/G37844.1

858 Palmer, C.D., Wittbrodt, P.R., 1991. Processes affecting the remediation of chromium-
859 contaminated sites. Environ. Health Perspect. 92, 25–40. doi:10.1289/ehp.919225

860 Partin, C.A., Lalonde, S.V., Planavsky, N.J., Bekker, A., Rouxel, O.J., Lyons, T.W.,
861 Konhauser, K.O., 2013. Uranium in iron formations and the rise of atmospheric
862 oxygen. Chem. Geol. 362, 82–90. doi:10.1016/j.chemgeo.2013.09.005

863 Planavsky, N.J., Reinhard, C.T., Wang, X., Thomson, D., McGoldrick, P., Rainbird, R.H.,
864 Johnson, T., Fischer, W.W., Lyons, T.W., 2014. Earth history. Low mid-Proterozoic
865 atmospheric oxygen levels and the delayed rise of animals. Science 346, 635–8.
866 doi:10.1126/science.1258410

867 Qin, L., Wang, X., 2017. Chromium Isotope Geochemistry. Rev. Mineral. Geochemistry
868 82, 379–414. doi:10.2138/rmg.2017.82.10

869 Raven, J.A., 1995. The early evolution of land plants: Aquatic ancestors and atmospheric
870 interactions. Bot. J. Scotl. 47, 151–175. doi:10.1080/03746609508684827

871 Rodler, A.S., Frei, R., Gaucher, C., Korte, C., Rosing, S.A., Germs, G.J.B., 2017.
872 Multiproxy isotope constraints on ocean compositional changes across the late
873 Neoproterozoic Ghaub glaciation, Otavi Group, Namibia. Precambrian Res. 298,
874 306–324. doi:10.1016/J.PRECAMRES.2017.05.006

875 Rovira, A.D., 1969. Plant root exudates. Bot. Rev. 35, 35–57. doi:10.1007/BF02859887

876 Ryan, B.M., Kirby, J.K., Degryse, F., Scheiderich, K., McLaughlin, M.J., 2014. Copper
877 Isotope Fractionation during Equilibration with Natural and Synthetic Ligands.
878 Environ. Sci. Technol. 48, 8620–8626. doi:10.1021/es500764x

879 Saad, E.M., Sun, J., Chen, S., Borkiewicz, O.J., Zhu, M., Duckworth, O.W., Tang, Y.,
880 2017a. Siderophore and Organic Acid Promoted Dissolution and Transformation of
881 Cr(III)-Fe(III)-(oxy)hydroxides. Environ. Sci. Technol. 51, 3223–3232.
882 doi:10.1021/acs.est.6b05408

883 Saad, E.M., Wang, X., Planavsky, N.J., Reinhard, C.T., Tang, Y., 2017b. Redox-
884 independent chromium isotope fractionation induced by ligand-promoted
885 dissolution. Nat. Commun. 8, 1590. doi:10.1038/s41467-017-01694-y

886 Schauble, E., Rossman, G.R., Taylor, H.P., 2004. Theoretical estimates of equilibrium
887 chromium-isotope fractionations. Chem. Geol. 205, 99–114.
888 doi:10.1016/j.chemgeo.2003.12.015

889 Schier, K., Bau, M., Münker, C., Beukes, N., Viehmann, S., 2018. Trace element and Nd
890 isotope composition of shallow seawater prior to the Great Oxidation Event:
891 Evidence from stromatolitic bioherms in the Paleoproterozoic Rooinekke and Nelani
892 Formations, South Africa. Precambrian Res. 315, 92–102.
893 doi:10.1016/J.PRECAMRES.2018.07.014

894 Schoenberg, R., Zink, S., Staubwasser, M., von Blanckenburg, F., 2008. The stable Cr
895 isotope inventory of solid Earth reservoirs determined by double spike MC-ICP-MS.
896 Chem. Geol. 249, 294–306. doi:10.1016/j.chemgeo.2008.01.009

897 Sikora, E.R., Johnson, T.M., Bullen, T.D., 2008. Microbial mass-dependent fractionation
898 of chromium isotopes. Geochim. Cosmochim. Acta 72, 3631–3641.
899 doi:10.1016/j.gca.2008.05.051

900 Smith, W.L., Raymond, K.N., 1979. The oxidation of uranium(IV) by N-
901 phenylbenzohydroxamic acid and the structure of the reaction product: Chlorodioxo-
902 N-phenylbenzohydroxamato-bis(Tetrahydrofuran)uranium(VI)[1]. J. Inorg. Nucl.
903 Chem. 41, 1431–1436. doi:10.1016/0022-1902(79)80206-7

904 Stewart, A.G., Hudson-Edwards, K.A., Dubbin, W.E., 2016. Effect of desferrioxamine B
905 and Suwannee River fulvic acid on Fe(III) release and Cr(III) desorption from
906 goethite. Geochim. Cosmochim. Acta 178, 62–75.
907 doi:doi.org/10.1016/j.gca.2015.11.047

908 Tanaka, K., Tani, Y., Takahashi, Y., Tanimizu, M., Suzuki, Y., Kozai, N., Ohnuki, T., 2010.
909 A specific Ce oxidation process during sorption of rare earth elements on biogenic
910 Mn oxide produced by Acremonium sp. strain KR21-2. Geochim. Cosmochim. Acta
911 74, 5463–5477. doi:10.1016/j.gca.2010.07.010

912 Teitzel, G.M., Geddie, A., De Long, S.K., Kirisits, M.J., Whiteley, M., Parsek, M.R., 2006.
913 Survival and growth in the presence of elevated copper: transcriptional profiling of
914 copper-stressed Pseudomonas aeruginosa. J. Bacteriol. 188, 7242–56.
915 doi:10.1128/JB.00837-06

916 Veglio', F., Beolchini, F., 1997. Removal of metals by biosorption: a review.
917 Hydrometallurgy 44, 301–316. doi:10.1016/S0304-386X(96)00059-X

918 Viehmann, S., Bau, M., Bühn, B., Dantas, E.L., Andrade, F.R.D., Walde, D.H.G., 2016.
919 Geochemical characterisation of Neoproterozoic marine habitats: Evidence from
920 trace elements and Nd isotopes in the Urucum iron and manganese formations,
921 Brazil. Precambrian Res. 282, 74–96. doi:10.1016/j.precamres.2016.07.006

922 Viehmann, S., Bau, M., Hoffmann, J.E., Münker, C., 2015. Geochemistry of the Krivoy
923 Rog Banded Iron Formation, Ukraine, and the impact of peak episodes of increased
924 global magmatic activity on the trace element composition of Precambrian
925 seawater. Precambrian Res. 270, 165–180.
926 doi:10.1016/J.PRECAMRES.2015.09.015

927 Voegelin, A.R., Nägler, T.F., Beukes, N.J., Lacassie, J.P., 2010. Molybdenum isotopes in
928 late Archean carbonate rocks: Implications for early Earth oxygenation.
929 Precambrian Res. 182, 70–82. doi:10.1016/j.precamres.2010.07.001

930 Wang, X., Planavsky, N.J., Reinhard, C.T., Zou, H., Ague, J.J., Wu, Y., Gill, B.C.,
931 Schwarzenbach, E.M., Peucker-Ehrenbrink, B., 2016. Chromium isotope
932 fractionation during subduction-related metamorphism, black shale weathering, and
933 hydrothermal alteration. Chem. Geol. 423, 19–33.
934 doi:10.1016/j.chemgeo.2016.01.003

935 Wanner, C., Eggenberger, U., Kurz, D., Zink, S., Mäder, U., 2012. A chromate-
936 contaminated site in southern Switzerland – Part 1: Site characterization and the
937 use of Cr isotopes to delineate fate and transport. Appl. Geochemistry 27, 644–654.
938 doi:10.1016/J.APGEOCHEM.2011.11.009

939 Watanabe, Y., Martini, J.E., Ohmoto, H., 2000. Geochemical evidence for terrestrial
940 ecosystems 2.6 billion years ago. Nature 408, 574–8. doi:10.1038/35046052

941 Watteau, F., Berthelin, J., 1994. Microbial dissolution of iron and aluminium from soil
942 minerals: efficiency and specificity of hydroxamate siderophores compared to
943 aliphatic acids. Eur. J. Soil Biol. 30, 1–9.

944 Wiederhold, J.G., 2015. Metal stable isotope signatures as tracers in environmental
945 geochemistry. Environ. Sci. Technol. 49, 2606–2624. doi:10.1021/es504683e

946 Wiederhold, J.G., Kraemer, S.M., Teutsch, N., Borer, P.M., Halliday, A.N., Kretzschmar,
947 R., 2006. Iron Isotope Fractionation during Proton-Promoted, Ligand-Controlled,
948 and Reductive Dissolution of Goethite. doi:10.1021/ES052228Y

949 Winkelmann, G., 1992. Structures and functions of fungal siderophores containing
950 hydroxamate and complexone type iron binding ligands. Mycol. Res. 96, 529–534.
951 doi:10.1016/S0953-7562(09)80976-3

952 Zink, S., Schoenberg, R., Staubwasser, M., 2010. Isotopic fractionation and reaction
953 kinetics between Cr(III) and Cr(VI) in aqueous media. Geochim. Cosmochim. Acta
954 74, 5729–5745. doi:10.1016/j.gca.2010.07.015

955 Zocher, A.-L., Kraemer, D., Merschel, G., Bau, M., 2018. Distribution of major and trace
956 elements in the bolete mushroom Suillus luteus and the bioavailability of rare earth
957 elements. Chem. Geol. 483, 491–500. doi:10.1016/J.CHEMGEO.2018.03.019

958

959 **Figures and Tables**

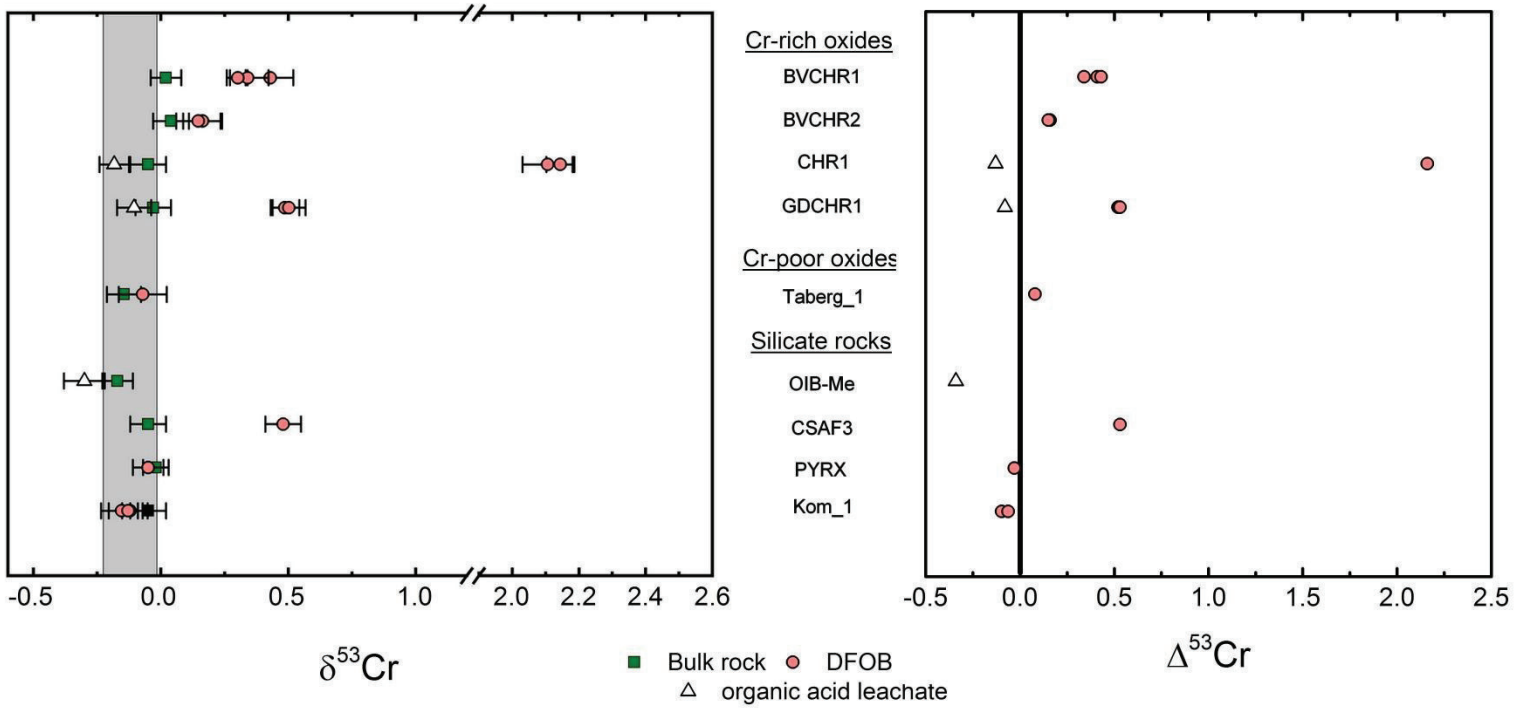

Fig. 1: Bulk rock $\delta^{53}Cr$, leachate $\delta^{53}Cr$ (left plot) and $\Delta^{53}Cr$ (right plot) obtained during the conducted leaching experiments. Note that the bulk rocks plot mostly inside the gray-shaded area which marks the extents of the high-temperature Cr isotope inventory (i.e., igneous rocks) (Schoenberg et al., 2008).

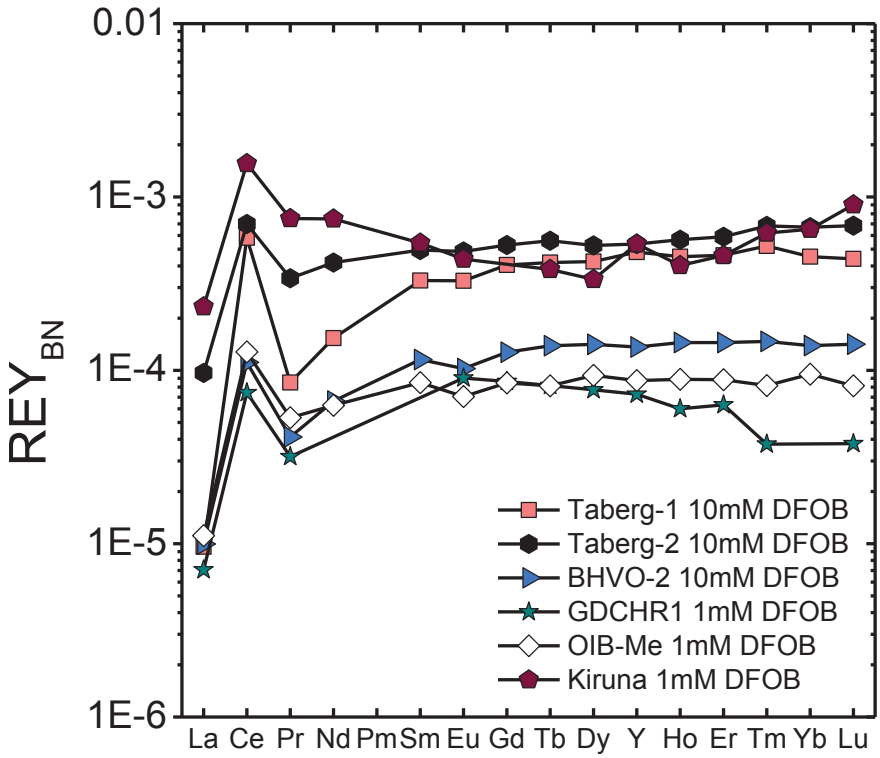

Fig. 2: Bulk rock-normalized REY patterns of the DFOB leachates where REY determination was possible. Note the decoupling of Ce from its LREY neighbors in all leachates, which indicates oxidation of Ce(III) to Ce(IV) during leaching in presence of the DFOB siderophore (Bau et al., 2013; Kraemer et al., 2015, 2016).

Tables

Table 1: Sample list, chromium concentrations and obtained bulk rock isotope data, analytical errors and number of conducted analyses on sample aliquots (n). Values marked with an asterisk obtained by portable XRF (Bruker S1 Titan, GeoChem Trace Program). Sample OIB-Me was described in detail as sample Me90-05 in Binard et al. (1993).

Sample	Description, Locality	[Cr] in mg kg^{-1} (* in wt.-%)	$\delta^{53}Cr_{bulk}$ (‰)	+/- 2s	n
Group I: Silicate rocks					
BHVO2	Hawaiian Basalt CRM, USGS	286	-0.12	0.07	4
OIB-Me	Ocean Island Basalt, Mehetia Hotspot	501	-0.17	0.06	7
CSAF3	Spheroidally weathered dolerite, Piet Retief, South Africa	2890	-0.05	0.07	5
PYRX	Bushveld Pyroxenite, Platreef Formation, South Africa	55421	-0.02	0.05	4
Kom1	Komatiite, Pioneer Creek Formation, Barberton Greenstone Belt, South Africa	1220	-0.063	0.036	4
Kom2	Komatiite, Pioneer Creek Formation, Barberton Greenstone Belt, South Africa	1240	-0.087	0.056	2
Group II: "Oxide" rocks					
BVCHR1	Chromitite, Bushveld Igneous Complex, South Africa	20.01 wt.-%*	0.02	0.06	5
BVCHR2	Chromitite, Bushveld Igneous Complex, South Africa	18.87 wt.-%*	0.04	0.07	5
CHR1	Chromitite, Bushveld Igneous Complex, South Africa	32.8 wt.-%*	-0.05	0.07	5
GDCHR1	Chromitite, Great Dyke, Zimbabwe	34.1 wt.-%*	-0.03	0.07	5
Taberg_1	Taberg Titanomagnetite	9.22	-0.15	0.067	3
Taberg_2	Taberg Titanomagnetite	9.21	-0.15	0.075	3
Mag_1a	Bushveld, upper main magnetite layer, South Africa	733	-0.098	0.067	3
Mag_1b	Bushveld, upper main magnetite layer, South Africa	406	-0.105	0.087	2
Kiruna	Kiruna Magnetite-Apatite Deposit	0.278	-0.092	0.087	2

975

Table 2: Chromium concentrations, isotope data and analytical errors of the siderophore and organic acid solutions after leaching of the respective rocks for 24 h on a shaker table at 180 rpm.						
Sample	**Reagent**	**Leachate pH after 24h**	**[Cr] in mg kg^{-1}**	**$\delta^{53}Cr_{leach}$ (‰)**	**+/- 2s**	$\Delta^{53}Cr$ (‰)
Group I: Silicate rocks						
BHVO2	1mM DFOB	7.0	0.0013	n/a	n/a	n/a
BHVO2	10mM DFOB	7.0	0.0140	n/a	n/a	n/a
OIB-Me	1mM DFOB	8.0	0.0033	n/a	n/a	n/a
OIB-Me	10mM citric acid	4.6	0.075	-0.30	0.10	-0.13
CSAF3	1mM DFOB	9	0.024	+0.48	0.07	+0.53
PYRX	1mM DFOB	7.9	0.019	-0.05	0.06	-0.03
Kom1	1mM DFOB	9.2	0.028	-0.16	0.086	-0.097
Kom2	1mM DFOB Replicate 1	9.4	0.0887	-0.15	0.081	-0.063
Kom2	1mM DFOB Replicate 2	9.4	0.0959	-0.12	0.031	-0.033
Group II: "Oxide" rocks						
BVCHR1	1mM DFOB Replicate 1	8.2	0.065	+0.43	0.09	+0.41
BVCHR1	1mM DFOB Replicate 2	7.6	0.0461	+0.34	0.082	+0.32
BVCHR1	1mM DFOB Replicate 1	not analysed	0.0443	+0.30	0.031	+0.28
BVCHR2	1mM DFOB Replicate 1	7.9	0.0071	+0.16	0.076	+0.12
BVCHR2	1mM DFOB Replicate 2	7.8	0.0065	+0.15	0.087	+0.11
CHR1	1mM DFOB Replicate 1	8.0	0.1046	+2.14	0.042	+2.19
CHR1	1mM DFOB Replicate 2	7.5	0.1083	+2.11	0.075	+2.16
CHR1	10mM citric acid	2.9	1.39	-0.18	0.058	-0.13
GDCHR1	1mM DFOB Replicate 1	7.3	0.0348	+0.49	0.056	+0.52
GDCHR1	1mM DFOB Replicate 2	7.8	0.0383	+0.50	0.065	+0.53
GDCHR1	10mM citric acid	2.9	0.4022	-0.11	0.067	-0.08
Taberg_1	1mM DFOB	9.8	0.0095	-0.071	0.094	+0.079
Taberg_2	1mM DFOB	9.5	< d.l.	n/a	n/a	n/a
Taberg_2	10mM DFOB	8.2	0.0055	n/a	n/a	n/a
Mag_1a	1mM DFOB Replicate 1	6.9	0.0014	n/a	n/a	n/a
Mag_1a	1mM DFOB Replicate 2	7.2	0.0013	n/a	n/a	n/a
Mag_1b	1mM DFOB	6.9	0.0016	n/a	n/a	n/a
Kiruna	1mM DFOB	8.6	0.0073	n/a	n/a	n/a

976

977

978

Table 3: Rare earth element and Y concentrations in DFOB leachates.						
Sample	**Taberg_1**	**Taberg_2**	**BHVO2**	**GDCHR Replicate 1**	**Kiruna**	**OIB-Me (Kraemer et al. 2015)**
Reagent	**1mM DFOB**	**1mM DFOB**	**10mM DFOB**	**1mM DFOB**	**1mM DFOB**	**1mM DFOB**
Analyte [ng kg^{-1}]						
La	34.4	373.7	154.3	3.4	1666.2	458
Ce	4866.2	6186.8	4233.1	80.3	15762.4	11439
Pr	96.1	407.6	230.5	5.1	635.5	610
Nd	750.3	2160.6	1627.2	29.8	1808.0	3071
Sm	339.6	533.6	692.4	10.8	166.1	893
Eu	160.7	275.0	215.0	3.1	10.8	228
Gd	413.7	543.7	839.2	10.2	n.d.	800
Tb	56.5	77.8	130.3	1.2	14.3	105
Dy	347.5	427.7	763.0	8.2	81.3	601
Y	1934.4	2137.2	3447.6	39.9	863.1	2356
Ho	70.6	88.5	141.7	1.5	21.8	94.1
Er	198.8	257.6	368.9	4.5	82.2	220
Tm	27.6	37.2	49.9	0.4	14.8	23.7
Yb	172.8	247.8	291.8	3.7	117.2	151
Lu	26.4	39.8	39.6	0.4	29.0	17.9

979